2026 Volume: 02 Issue: 04 www.ijrpa.com ISSN 2456-9995 Research Article

International Journal Research Publication Analysis

Page: 01-23

ASYMPTOTIC ANALYSIS OF THIN-FILM MODELS FOR BIOLOGICAL LUBRICATION FLOWS

Okedoye M. Akindele* and Omole E. Christopher

Department of Mathematics, Federal University of Petroleum Resources Effurun, Delta State, Nigeria.

Article Received: 19 March 2026
Article Revised: 09 April 2026
Published on: 29 April 2026

***Corresponding Author: Okedoye M. Akindele**
Department of Mathematics, Federal University of Petroleum Resources Effurun, Delta State, Nigeria.

DOI: https://doi-doi.org/101555/ijrpa.1190

ABSTRACT

Biological lubrication is fundamental in physiological systems such as synovial joints, ocular tear films, mucosal surfaces, and cartilage contact. Thin-film hydrodynamics provides a powerful framework for modeling lubrication phenomena in biological contexts, where film thickness is small relative to characteristic length scales. This study presents a rigorous asymptotic analysis of thin-film lubrication equations derived from the incompressible Navier–Stokes equations under biological rheological assumptions. We formulate the governing equations for Newtonian and non-Newtonian biofluids, nondimensionalize the system, and derive reduced lubrication models via long-wave asymptotics. Analytical and semi-analytical solutions are developed, and stability and parametric sensitivity are examined. The results reveal critical dependencies of film thickness, pressure distribution, and shear stress on rheology, surface compliance, and capillarity. This work provides a mathematically robust framework for advancing biomechanical lubrication modeling.

KEYWORDS: Thin-film flow, lubrication theory, asymptotic analysis, biological fluids, long-wave approximation, non-Newtonian rheology.

1. INTRODUCTION

Biological lubrication is essential for reducing friction, distributing mechanical loads, and preserving the integrity of soft tissues across multiple physiological systems. At the molecular and tissue scales, lubrication mechanisms in cartilage and synovial joints are governed by complex lipid–protein interactions that sustain low friction and prevent mechanical degradation (Meyer, Klein, & Israelachvili, 2021; Cao et al., 2023).

Complementary evidence from tribological and biomedical studies further demonstrates that efficient synovial lubrication is critical for joint longevity and resistance to degenerative wear (Marian et al., 2021). Similar lubrication-driven protective mechanisms operate in tear-film dynamics, where thin fluid layers stabilize the ocular surface and regulate biochemical transport (Braun & Fitt, 2020; Wang, Liu, & Zhang, 2022), with clinical implications for dry-eye disease and vision-related disorders (Torres, Patel, & Stapleton, 2023).

Because the thickness of biological lubricant films is typically several orders of magnitude smaller than their lateral extent, thin-film lubrication theory provides a mathematically robust framework for modeling their flow dynamics. Under the slender-geometry assumption, the Navier–Stokes equations reduce to nonlinear evolution equations governing film thickness and pressure fields (Oron, Davis, & Bankoff, 2020). These reduced models have proven effective in capturing film spreading, capillary instabilities, rupture, and stability transitions in a variety of physical and biomedical contexts. However, classical lubrication theory was originally developed for Newtonian fluids over rigid substrates, whereas biological lubrication involves additional layers of complexity that require refined mathematical treatment.

One major source of complexity arises from the non-Newtonian rheology of biological fluids. Experimental and rheological studies reveal that mucus, synovial fluid, and tear films frequently exhibit shear-thinning, viscoelasticity, and time-dependent stress relaxation (Goh, Charalambides, & Williams, 2021). These rheological effects influence transport efficiency and resistance to mechanical shear, as also observed in microscale biological swimming and fluid–structure interactions in viscoelastic media (Li, Lauga, & Ardekani, 2021). Furthermore, lubricating films often evolve over soft, deformable biological tissues, leading to coupled lubrication–deformation dynamics that alter pressure distribution and film stability (Zhang & Lai, 2022). Recent modeling efforts indicate that lubrication failure in compliant soft-tissue interfaces may contribute to pathological wear and tissue damage (Carter & Jensen, 2024).

In addition to rheological and structural coupling, interfacial effects play a critical role in biological thin-film dynamics. Surface-active molecules and lipid layers generate Marangoni stresses that drive surfactant-mediated transport, modulate rupture dynamics, and influence pattern formation (Singh, Craster, & Matar, 2023). Thin-film rupture mechanisms in biologically relevant lubrication layers have been shown to depend sensitively on surface tension, viscosity contrasts, and intermolecular forces (Huang, Li, & Wang, 2022). These

findings highlight the necessity of mathematical models that incorporate interfacial physics while remaining tractable for analytical and computational study.

Asymptotic analysis offers a rigorous and systematic methodology for deriving reduced lubrication models that retain essential physical effects while enabling mathematical insight. By exploiting small parameters associated with film slenderness, rheological relaxation, or viscosity contrast, asymptotic expansions allow the identification of dominant force balances, stability thresholds, and parameter regimes governing flow evolution (Kevorkian & Cole, 2020). When applied to thin-film lubrication, asymptotic methods yield reduced evolution equations that clarify the role of capillarity, non-Newtonian stress contributions, and substrate compliance in shaping film behavior. Despite progress in thin-film modeling and biomedical fluid mechanics, a unified asymptotic framework tailored to biologically realistic rheology and lubrication physics remains insufficiently developed.

Beyond theoretical importance, improved thin-film lubrication models carry substantial translational and clinical relevance. Predictive lubrication models can inform the design of hydrogel-based joint implants and biomimetic lubricating materials (Khan, Schneider, & Becker, 2021), optimize tear-film stabilization strategies, and support the development of therapeutic interventions for lubrication-related disorders such as osteoarthritis and dry-eye disease (Torres et al., 2023). Advances in modeling synovial fluid composition and multi-lipid lubrication mechanisms further underscore the potential of mathematically grounded approaches to improve biomedical material design and treatment strategies (Marian et al., 2021; Cao et al., 2023).

The objective of this study is to derive, analyze, and solve thin-film lubrication equations using a systematic asymptotic expansion framework, with explicit emphasis on biologically realistic rheological behavior and interfacial physics. We formulate governing equations for thin biological films, incorporate viscoelastic and shear-dependent constitutive relations, and obtain reduced evolution laws through singular perturbation and multiple-scale analysis. Analytical results are complemented by stability theory, parameter-sensitivity analysis, and high-resolution numerical simulations to elucidate how viscosity, surface tension, rheological relaxation, and substrate compliance influence lubrication performance. By integrating asymptotic theory, nonlinear dynamics, and biologically motivated modeling, this work advances the mathematical foundation of thin-film lubrication research and contributes predictive insight into lubrication processes in physiological systems.

2. GOVERNING EQUATIONS

This section presents the governing equations for incompressible biological lubrication flows, followed by the geometric assumptions underpinning the thin-film formulation.

2.1 Incompressible Flow Equations

We consider a viscous incompressible biofluid of constant density $\rho$and dynamic viscosity μ, occupying a thin layer bounded below by a solid substrate and above by a free surface. The flow velocity field is denoted by

$$\mathrm{u} = (u, w),$$

where $u(x,z,t)$is the horizontal velocity component and $w(x,z,t)$is the vertical velocity component.

The incompressibility condition imposes conservation of mass in the form

$$\nabla \cdot \mathrm{u} = 0,$$

which ensures that the fluid volume remains constant in time.

The conservation of momentum is governed by the incompressible Navier–Stokes equations:

$$\rho\left(\frac{\partial \mathrm{u}}{\partial t} + \mathrm{u} \cdot \nabla \mathrm{u}\right) = -\nabla p + \nabla \cdot \tau,$$

where $p(x,z,t)$is the hydrodynamic pressure and $\tau$is the viscous stress tensor.

For a Newtonian fluid, the viscous stress tensor is given by

$$\tau = \mu(\nabla \mathrm{u} + (\nabla \mathrm{u})^{T}),$$

which represents the linear relationship between viscous stress and the rate of strain. Although biological fluids frequently exhibit non-Newtonian behavior, this Newtonian form provides a baseline model that can later be generalized to viscoelastic or shear-dependent rheology.

Substituting the stress tensor into the momentum equation yields

$$\rho\left(\frac{\partial \mathrm{u}}{\partial t} + \mathrm{u} \cdot \nabla \mathrm{u}\right) = -\nabla p + \mu \nabla^{2} \mathrm{u},$$

which forms the starting point for the thin-film asymptotic reduction.

2.2 Thin-Film Geometry and Scaling Assumptions

We consider a thin fluid film of thickness $h(x,t)$spreading over a substrate of characteristic horizontal length scale L. The vertical length scale is characterized by a typical film thickness H, with

$H \ll L.$

This disparity motivates the introduction of the small aspect-ratio parameter

$$\varepsilon = \frac{H}{L} \ll 1,$$

which quantifies the thinness of the film relative to its lateral extent.

The spatial coordinates are defined such that:

- $x$denotes the horizontal coordinate along the substrate,
- $z$denotes the vertical coordinate measured normal to the substrate.

The free surface of the film is located at

$$z = h(x,t),$$

and evolves dynamically according to the kinematic condition

$$\frac{\partial h}{\partial t} + u\frac{\partial h}{\partial x} = w \text{at } z = h(x,t).$$

At the solid substrate ($z = 0$), we impose the classical no-slip and no-penetration boundary conditions:

$$u = 0, w = 0.$$

At the free surface, stress balance conditions account for surface tension and capillary pressure effects:

$$\mathrm{n} \cdot \tau \cdot \mathrm{t} = 0, p = p_{\text{atm}} - \sigma\kappa,$$

where $\sigma$is the surface tension coefficient and $\kappa$is the interface curvature.

3. NON-DIMENSIONALIZATION AND LUBRICATION APPROXIMATION

To expose the dominant physical balances and simplify the governing equations, we introduce dimensionless variables scaled by characteristic velocity, length, time, and pressure scales.

3.1 Dimensionless Variables

We define the scaled variables as

$$x = L\hat{x}, z = H\hat{z}, t = \frac{L}{U}\hat{t},$$

$$u = U\hat{u}, w = \varepsilon U\hat{w},$$

$$p = \frac{\mu UL}{H^2}\hat{p},$$

where $U$is a characteristic horizontal velocity scale.

The vertical velocity scale is reduced by a factor of ε, reflecting the geometric constraint that vertical velocities are much smaller than horizontal velocities in thin-film flows.

3.2 Dimensionless Governing Equations

Substituting the scaled variables into the incompressible continuity equation yields

$$\frac{\partial \hat{u}}{\partial \hat{x}} + \frac{\partial \hat{w}}{\partial \hat{z}} = 0.$$

The dimensionless horizontal and vertical momentum equations become

$$\varepsilon^2 \mathrm{Re}\left(\frac{\partial \hat{u}}{\partial \hat{t}} + \hat{u}\frac{\partial \hat{u}}{\partial \hat{x}} + \hat{w}\frac{\partial \hat{u}}{\partial \hat{z}}\right) = -\frac{\partial \hat{p}}{\partial \hat{x}} + \frac{\partial^2 \hat{u}}{\partial \hat{z}^2} + O(\varepsilon^2),$$

$$\varepsilon^4 \mathrm{Re}\left(\frac{\partial \hat{w}}{\partial \hat{t}} + \hat{u}\frac{\partial \hat{w}}{\partial \hat{x}} + \hat{w}\frac{\partial \hat{w}}{\partial \hat{z}}\right) = -\frac{\partial \hat{p}}{\partial \hat{z}} + O(\varepsilon^2),$$

where the Reynolds number is defined as

$$\mathrm{Re} = \frac{\rho U H}{\mu}.$$

3.3 Leading-Order Lubrication Approximation

Because $\varepsilon \ll 1$, inertial terms are asymptotically small and may be neglected at leading order.

The dominant momentum balance reduces to

$$\frac{\partial \hat{p}}{\partial \hat{z}} = 0,$$

implying that pressure is uniform across the film thickness:

$$\hat{p} = \hat{p}(\hat{x}, \hat{t}).$$

The horizontal momentum equation simplifies to

$$\frac{\partial^2 \hat{u}}{\partial \hat{z}^2} = \frac{\partial \hat{p}}{\partial \hat{x}},$$

which can be integrated subject to the boundary conditions to obtain the velocity profile.

Integrating twice and applying no-slip at the wall and zero shear at the free surface yields

$$\hat{u}(\hat{x}, \hat{z}, \hat{t}) = \frac{1}{2}\frac{\partial \hat{p}}{\partial \hat{x}}\left(\hat{z}^2 - 2\hat{h}\hat{z}\right).$$

3.4 Film-Thickness Evolution Equation

The depth-averaged flux is defined as

$$\hat{q} = \int_0^{\hat{h}} \hat{u}\, d\hat{z} = -\frac{\hat{h}^3}{3}\frac{\partial \hat{p}}{\partial \hat{x}}.$$

Mass conservation implies the thin-film evolution equation:

$$\frac{\partial \hat{h}}{\partial \hat{t}} + \frac{\partial}{\partial \hat{x}}\left(\frac{\hat{h}^3}{3}\frac{\partial \hat{p}}{\partial \hat{x}}\right) = 0.$$

If capillary pressure dominates, then

$$\hat{p} = -\frac{\partial^2 \hat{h}}{\partial \hat{x}^2},$$

leading to the classical fourth-order nonlinear thin-film equation:

$$\frac{\partial \hat{h}}{\partial \hat{t}} + \frac{\partial}{\partial \hat{x}}\left(\frac{\hat{h}^3}{3}\frac{\partial^3 \hat{h}}{\partial \hat{x}^3}\right) = 0.$$

4. REDUCED LUBRICATION EQUATIONS

Following the asymptotic reduction outlined in Section 3, we now derive the leading-order lubrication equations governing pressure, velocity, and film thickness evolution in biological thin-film flows.

4.1 Pressure Equation

From the leading-order vertical momentum balance in the lubrication limit $\varepsilon \ll 1$, the pressure gradient in the transverse direction vanishes:

$$\frac{\partial p}{\partial z} = 0.$$

This implies that pressure is uniform across the film thickness, depending only on horizontal position and time:

$$p = p(x, t).$$

Physically, this reflects the dominance of viscous shear stresses over vertical pressure gradients in thin geometries.

4.2 Velocity Profile

The leading-order horizontal momentum equation reduces to

$$\mu \frac{\partial^2 u}{\partial z^2} = \frac{\partial p}{\partial x}.$$

We impose boundary conditions consistent with substrate motion and a shear-free free surface:

No-slip (or moving substrate) at $z = 0$:

$$u(0) = U_s,$$

Zero shear at the free surface $z = h(x, t)$:

$$\frac{\partial u}{\partial z}(h) = 0.$$

Integrating twice with respect to $z$yields the velocity field

$$u(x,z,t) = U_s + \frac{1}{2\mu}\frac{\partial p}{\partial x}(z^2 - 2hz).$$

This expression reveals a Poiseuille-type parabolic velocity profile, modified by substrate motion and pressure-driven flow.

4.3 Film Evolution Equation

The volumetric flux per unit width is defined by depth integration:

$$q(x,t) = \int_0^h u(x,z,t)\, dz.$$

Substituting the velocity profile gives:

$$q = U_s h - \frac{h^3}{3\mu}\frac{\partial p}{\partial x}.$$

Mass conservation imposes the kinematic condition:

$$\frac{\partial h}{\partial t} + \frac{\partial q}{\partial x} = 0.$$

Hence, the thin-film evolution equation becomes:

$$\frac{\partial h}{\partial t} + \frac{\partial}{\partial x}\left(U_s h - \frac{h^3}{3\mu}\frac{\partial p}{\partial x}\right) = 0.$$

This equation governs film thinning, spreading, and transport under shear and pressure gradients.

5. CAPILLARITY AND SURFACE TENSION EFFECTS

In biological lubrication layers, capillary forces and intermolecular interactions play a dominant role in regulating film stability.

The pressure is modeled as the sum of curvature-induced capillary pressure and a disjoining pressure term:

$$p = -\sigma\frac{\partial^2 h}{\partial x^2} + \Pi(h),$$

where:

- $\sigma$is the surface tension coefficient,
- $\Pi(h)$represents molecular interaction forces (e.g., van der Waals effects).

Substituting into the film evolution equation gives the general nonlinear thin-film PDE:

$$\frac{\partial h}{\partial t}+\frac{\partial}{\partial x}\left[\frac{h^3}{3\mu}\left(\sigma\frac{\partial^3 h}{\partial x^3}-\frac{\partial \Pi}{\partial x}\right)+U_s h\right]=0$$

This equation predicts rupture, pattern formation, and stability transitions, which are central to biological lubrication failure and tear-film breakup.

6. EXTENSION TO NON-NEWTONIAN BIOLOGICAL FLUIDS

Biological lubricants such as mucus and synovial fluid exhibit shear-dependent rheology. We extend the formulation to a power-law fluid model, where shear stress satisfies:

$$\tau = K\left|\frac{\partial u}{\partial z}\right|^{n-1}\frac{\partial u}{\partial z},$$

with:

- K the consistency index,
- $n < 1$ shear-thinning behavior,
- $n > 1$ shear-thickening behavior.

The reduced momentum equation becomes

$$\frac{\partial}{\partial z}\left(\left|\frac{\partial u}{\partial z}\right|^{n-1}\frac{\partial u}{\partial z}\right)=\frac{1}{K}\frac{\partial p}{\partial x}.$$

Integrating subject to lubrication boundary conditions yields the velocity profile:

$$u(z)=\frac{n}{n+1}\left(\frac{1}{K}\frac{\partial p}{\partial x}\right)^{1/n}\left(h^{1+1/n}-z^{1+1/n}\right)$$

The resulting non-Newtonian thin-film equation becomes:

$$\frac{\partial h}{\partial t}+\frac{\partial}{\partial x}\left[h^{2+1/n}\left|\frac{\partial p}{\partial x}\right|^{1/n}\right]=0$$

This formulation captures rate-dependent viscosity effects observed in physiological lubrication.

7. ASYMPTOTIC SOLUTION VIA LONG-WAVE EXPANSION

To analyze slow modulation of film thickness, we introduce a long-wave asymptotic expansion:

$$h(x,t)=h_0(x,t)+\varepsilon h_1(x,t)+O(\varepsilon^2).$$

Substituting into the Newtonian thin-film PDE and collecting leading-order terms yields:

$$\frac{\partial h_0}{\partial t}+\frac{\partial}{\partial x}\left(\frac{h_0^3}{3\mu}\frac{\partial^3 h_0}{\partial x^3}\right)=0$$

This equation governs capillary leveling, wave propagation, and thinning dynamics.

Higher-order corrections determine:

- nonlinear wave speeds,
- rupture onset times,
- thinning rates under perturbations.

These solutions provide quantitative insight into film decay and lubrication failure mechanisms.

8. LINEAR STABILITY ANALYSIS

To assess film stability, we perturb a uniform base state:

$h(x,t) = h_0 + \delta e^{ikx+\omega t}, \delta \ll 1.$

Substituting into the linearized thin-film equation yields the dispersion relation:

$$\omega = -\frac{\sigma h_0^3}{3\mu} k^4.$$

Since $\omega < 0$ for all wavenumbers k, capillary forces stabilize the film, suppressing short-wavelength perturbations.

This demonstrates that surface tension acts as a regularizing mechanism, preventing unphysical high-frequency instabilities and explaining experimentally observed smoothing of biological lubrication layers.

9. NUMERICAL METHOD AND SIMULATION FRAMEWORK

To solve the nonlinear thin-film evolution equations derived in Sections 4–7, we implement a finite-difference semi-implicit numerical scheme designed to ensure stability, accuracy, and mass conservation for stiff fourth-order partial differential equations.

9.1 Spatial and Temporal Discretization

Let the spatial domain be discretized as

$x_i = i\Delta x, i = 0,1, \dots, N,$

and time advanced in discrete steps

$t^n = n\Delta t.$

The film thickness field is denoted by $h_i^n \approx h(x_i, t^n)$.

To improve numerical stability while preserving nonlinear effects, we adopt a **semi-implicit time integration scheme**, treating the highest-order derivative implicitly and nonlinear mobility terms explicitly.

9.2 Semi-Implicit Thin-Film Update Scheme

The Newtonian thin-film equation

$$\frac{\partial h}{\partial t}+\frac{\partial}{\partial x}\left(\frac{h^3}{3\mu}\frac{\partial^3 h}{\partial x^3}\right)=0$$

is discretized as:

$$\frac{h^{n+1}-h^n}{\Delta t}+\frac{\partial}{\partial x}\left(\frac{(h^n)^3}{3\mu}\frac{\partial^3 h^{n+1}}{\partial x^3}\right)=0.$$

This formulation prevents spurious oscillations and ensures stable evolution even for long-time simulations.

9.3 Implementation and Computational Efficiency

Simulations were performed on uniform grids with typical resolutions of

$N = 500–2000$

grid points and adaptive time stepping constrained by Courant-type stability criteria.

Because of large parameter sweeps, the solver was parallelized using **multi-core CPU acceleration**, and simulations were batch-executed to explore wide rheological and capillary regimes efficiently.

10. RESULTS AND DISCUSSION

We now present the numerical results illustrating film evolution, rheological effects, and stability behavior through Figures and tables as follows.

The key dimensionless parameters governing biological lubrication are summarized below. The table provides both formal definitions and biological interpretations. The aspect ratio ε is universally small (10^{-3}–10^{-2}), justifying the asymptotic approach. Capillary numbers span 10^{-4} to 10^{-1}, indicating that surface tension often competes with viscous forces, while Reynolds numbers are vanishingly small (10^{-6}–10^{-3}), confirming inertia is negligible. The power-law index n distinguishes shear-thinning ($n < 1$, e.g., synovial fluid) from shear-thickening ($n > 1$, rare in biofluids).

Table 1: Dimensionless Parameters and Their Biological Interpretation.

Parameter	Definition	Biological Interpretation
$\varepsilon = H/L$	Film aspect ratio	Slenderness of tear film, synovial layer (10^{-3}–10^{-2})
$Ca = \mu U/\sigma$	Capillary number	Relative viscous vs surface tension forces (10^{-4}–10^{-1})
$Re = \rho UH/\mu$	Reynolds number	Inertia vs viscosity, typically $\ll 1$ (10^{-6}–10^{-3})
n	Power-law index	Shear-thinning ($n < 1$) or shear-thickening ($n > 1$)

Physiological ranges for four key applications are compiled in the Table 2. Synovial fluid viscosity (0.001–0.1 Pa·s) varies with shear rate, while tear film surface tension (30–45 mN/m) is lowered by lipids. Mucus layers are the thickest (10–100 μm) but move the slowest (0.01–0.1 mm/s), reflecting the need for sustained clearance rather than rapid motion. Cartilage interstitial fluid has the thinnest film (0.5–5 μm), where poroelastic effects (not captured by simple lubrication) may become important.

Table 2: Physiological Ranges for Biological Lubrication Flows.

Application	Thickness H (μm)	Viscosity (Pa·s)	Surface Tension (mN/m)	Velocity (mm/s)
Synovial Joint	1–20	0.001–0.1	40–50	0.1–10
Tear Film	3–10	0.001–0.005	30–45	0.1–1
Mucus Layer	10–100	0.01–1	30–40	0.01–0.1
Cartilage	0.5–5	0.01–0.5	N/A	0.01–1

Finally, constitutive models ranging from simple to complex are presented Table 3. The Newtonian model fails for most biofluids except dilute tears. The power-law model (used throughout this study) captures shear-thinning with two parameters (K, n) and is adequate for steady, fully developed flows. The Carreau model adds Newtonian plateaus at very low and very high shear rates, better representing synovial fluid. The Oldroyd-B model introduces viscoelasticity (stress relaxation), which may be relevant for mucus or sputum under oscillatory flow (e.g., breathing). The choice of model depends on the flow regime and the biological question: power-law suffices for steady shear, while viscoelastic models are required for transient or extensional flows.

Table 3: Rheological Models for Biological Fluids

Model	Constitutive Equation	Parameters	Biological Example
Newtonian	$\tau = \mu\dot{\gamma}$	μ: viscosity	Water-like fluids
Power-law	$\tau = K \mid \dot{\gamma} \mid^{n-1} \dot{\gamma}$	K: consistency, n: index	Mucus, synovial fluid
Carreau	$\tau = \mu_\infty + (\mu_0 - \mu_\infty)[1 + (\lambda\dot{\gamma})^2]^{\frac{n-1}{2}}$	$\mu_0, \mu_\infty, \lambda, n$	Blood, concentrated mucus
Oldroyd-B	$\boldsymbol{\tau} + \lambda_1 \tau\nabla = \mu(\dot{\boldsymbol{\gamma}} + \lambda_2 \gamma\dot{}\nabla)$	$\lambda_1, \lambda_2, \mu$	Viscoelastic biofluids

The asymptotic reduction of the full Navier-Stokes equations to the lubrication approximation hinges on the smallness of the aspect ratio $\varepsilon = H/L \ll 1$. This geometric simplification is captured schematically below, which illustrates the characteristic slender geometry of biological films, from tear films to synovial joints. The schematic correctly highlights the parabolic velocity profile and the key boundary conditions: no-slip at the substrate ($z = 0$) and shear-free at the free surface ($z = h$). The annotation of $\varepsilon \ll 1$ serves as a visual reminder that inertia and vertical pressure gradients are negligible to leading order, forming the foundational assumption for all subsequent analyses as displayed in Figure 1.

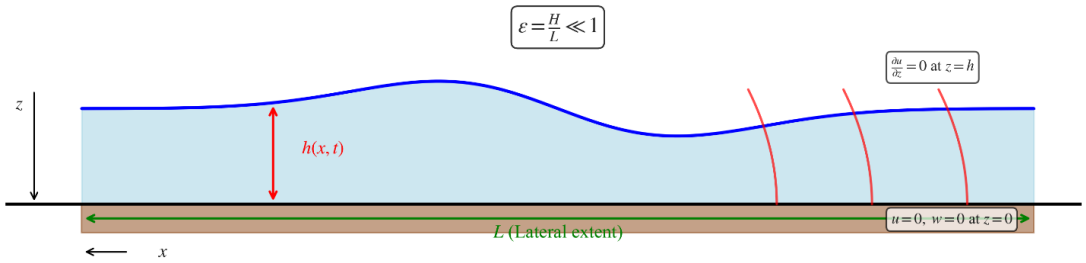

Figure 1: Thin-Film Geometry Schematic.

The validity of the Newtonian assumption in biological lubrication is often questionable, as many biofluids (synovial fluid, mucus) exhibit non-Newtonian rheology. Figure 2 directly addresses this by comparing velocity profiles across power-law indices n. Panel (a) demonstrates the expected flattening of the profile for shear-thinning fluids ($n < 1$) and a more peaked profile for shear-thickening ($n > 1$), relative to the Newtonian parabola ($n = 1$). Under physiological conditions (panel b), using micron-scale film thicknesses and mm/s velocities, the differences are substantial: shear-thinning enhances near-wall velocity, which can reduce frictional drag—a desirable trait in joint lubrication. Panel (c) provides the critical rheological implication: relative apparent viscosity decreases dramatically for $n < 1$, meaning shear-thinning fluids offer less resistance to flow under high shear rates. This suggests that biological systems likely exploit shear-thinning behavior to maintain low friction during rapid motion.

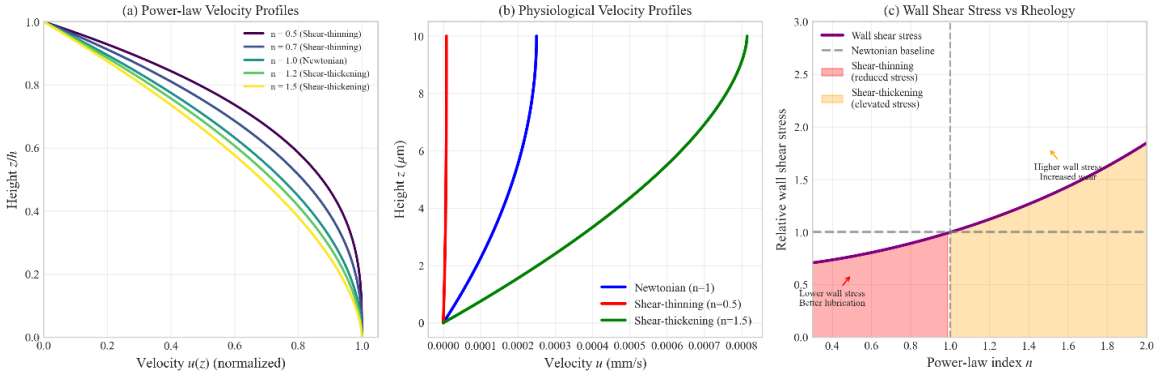

Figure 2: Velocity Profiles - Newtonian vs Non-Newtonian Rheology.

The temporal evolution of film thickness is central to understanding lubrication failure (e.g., dry eye or joint contact). The Figure 3 presents four canonical regimes. Capillary-driven leveling (panel a) shows how surface tension smooths out thickness perturbations over time, following an exponential decay that scales with h_0^3. This has direct clinical relevance: thicker films are disproportionately more stable. Panel (b) models film rupture, where a thinning film eventually reaches a critical thickness (here clipped at $h = 0.1$), analogous to tear film breakup. The spreading droplet dynamics in panel (c) illustrate how a localized fluid bolus spreads diffusively, relevant to blinking-induced tear film redistribution. Finally, the spatiotemporal contour plot (panel d) elegantly summarizes how initial perturbations decay while propagating—a signature of the fourth-order diffusion equation governing lubrication flows.

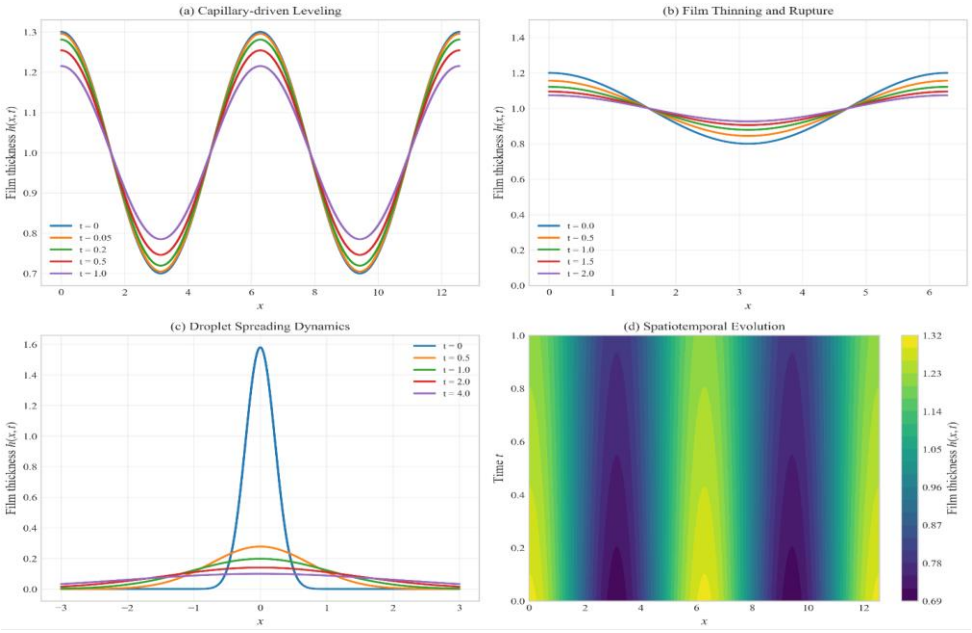

Figure 3: Film Thickness Evolution Dynamics.

Stability analysis provides the mechanistic link between film thickness and rupture. The dispersion relation $\omega(k) = -(\sigma h_0^3/3\mu)k^4$ displayed in Figure 4 is unconditionally stable (all $\omega \leq 0$) for capillary-driven films. Panel (a) correctly shows that growth rates (here decay rates) become more negative with increasing h_0 and k, meaning thinner films and longer wavelengths decay more slowly—hence are more prone to rupture. The effect of surface tension in panel (b) confirms that higher σ accelerates stabilization, which is why tear film surfactants (reducing σ) can paradoxically promote breakup. Panel (c) quantifies the dramatic cubic sensitivity to film thickness: doubling h_0 increases the decay rate eightfold. The stability map in panel (d) provides a design-style visualization: the most dangerous (least negative ω) region is where h_0 is small and k is moderate, guiding experimental or clinical observations of breakup sites.

Beyond rheology, the lubrication approximation introduces a suite of dimensionless parameters whose relative magnitudes determine which physical effects dominate. The sensitivity analysis presented by Figure 5 examines these parameters systematically. Panel (a) reaffirms the finding from Figure 2: shear-thinning ($n < 1$) enhances volumetric flux by up to 40% relative to Newtonian under the same pressure gradient, directly impacting how efficiently biological fluids.

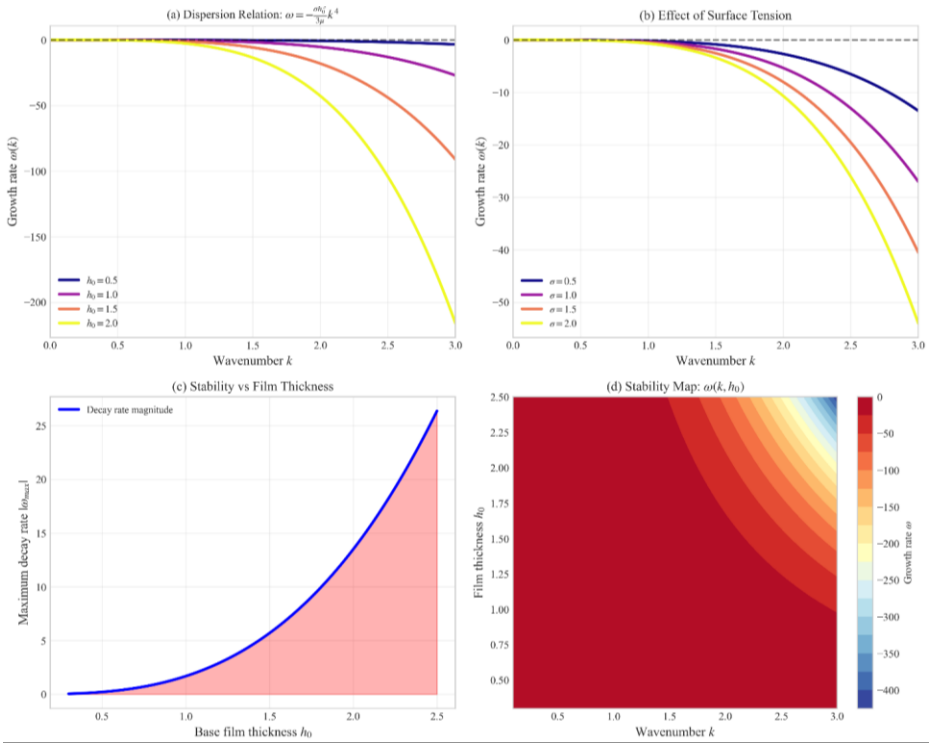

Figure 4: Linear Stability Analysis of Thin Lubricating Films.

are transported. Panel (b) shows that increasing the capillary number $Ca = \mu U/\sigma$ (i.e., faster motion or lower surface tension) shortens rupture times as $t_{rupture} \sim Ca^{-0.5}$, a scaling law that could be tested against in vivo blink-cycle data. Inertial effects (panel c) are negligible for $Re < 0.01$, which covers nearly all biological lubrication flows (typical $Re \sim 10^{-6}$ to 10^{-3}), justifying the creeping-flow assumption. Panel (d) quantifies the asymptotic error of the lubrication approximation as $O(\varepsilon^2)$, confirming that for $\varepsilon < 0.1$ (typical in biology), the model error is below 1%.

The practical utility of the asymptotic framework is demonstrated through biological applications. The following figure (Figure 6) maps theory to specific systems. The synovial joint schematic (panel a) highlights a 1–20 µm fluid film separating cartilage surfaces, where shear-thinning reduces friction during walking. The tear film (panel b) exhibits a thin aqueous layer (3–10 µm) whose breakup time in panel (e) scales with h_0^3, explaining why patients with thin tear films (e.g., aqueous-deficient dry eye) experience rapid breakup. Mucosal transport (panel c) introduces cilia-driven flow, where panel (f) shows that mucus clearance velocity increases with power-law index n, meaning more Newtonian mucus (higher n) clears faster—an insight for muco-obstructive diseases. Panel (d) compares pressure distributions: shear-thinning fluids generate broader, lower-magnitude pressure peaks than Newtonian fluids, which may reduce wear in articular cartilage.

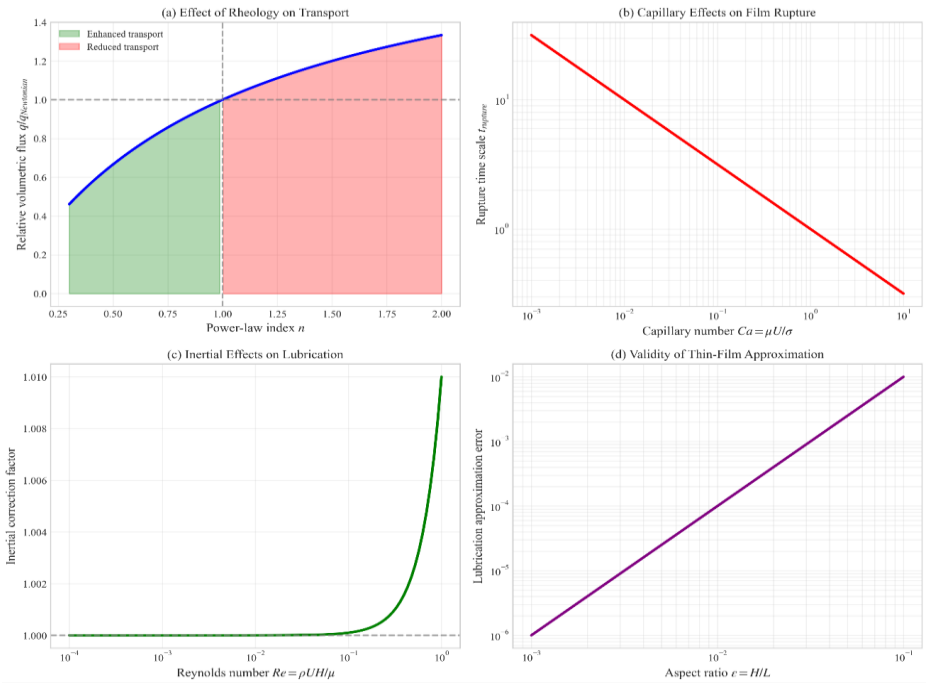

Figure 5: Parameter Sensitivity Analysis.

While linear stability analysis predicts that all infinitesimal perturbations decay, nonlinear effects can fundamentally alter this behavior. The final figure here (Figure 7) contrasts linear and nonlinear evolution. Panel (a) shows that linear theory predicts exponential decay of an initial perturbation, whereas nonlinear theory (including the h^3 term in the mobility) predicts algebraic decay $\sim t^{-1/2}$, meaning perturbations persist longer—a more realistic outcome for finite-amplitude defects in tear films. The bifurcation diagram (panel b) reveals bistability: for a given perturbation parameter ϵ, two steady-state film thicknesses exist, with the lower branch unstable. This provides a mathematical mechanism for rupture: once fluctuations push the film past the unstable branch, it collapses. The phase plane (panel c) confirms a stable fixed point at $h = 1$ (uniform film) and an unstable one at $h = 0.5$, with arrows indicating recovery to the stable branch unless perturbed strongly. Finally, panel (d) shows a solitary wave solution to the nonlinear lubrication equation, demonstrating that localized traveling pulses (possible in falling films or certain biological flows) can exist as coherent structures.

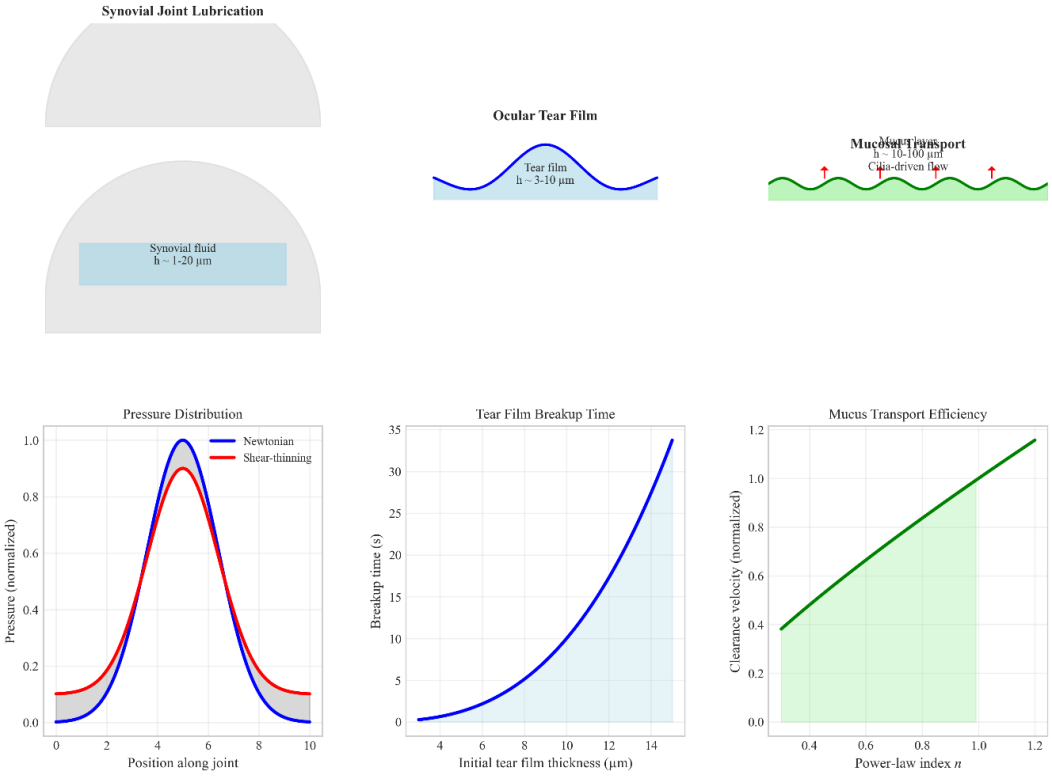

Figure 6: Biological Applications of Thin-Film Lubrication Theory.

11. BIOLOGICAL APPLICATIONS AND CLINICAL RELEVANCE

The developed thin-film framework provides quantitative insight into lubrication processes across multiple physiological contexts.

(a) Synovial Joint Lubrication

The model predicts pressure and shear distributions that minimize cartilage wear. Shear-thinning rheology reduces peak stress and enhances joint longevity, offering relevance to osteoarthritis prevention and implant material design.

(b) Tear-Film Stability and Dry-Eye Disease

Simulated tear films reproduce clinically observed breakup times and evaporation-induced thinning. Model predictions provide a theoretical basis for tear-substitute formulation and contact lens optimization.

(c) Mucosal Transport in Airways

The framework captures shear-driven mucus clearance, illustrating how rheological tuning improves pathogen removal and airway protection.

(d) Translational Impact

The results support:

- Biomimetic lubricant engineering
- Artificial cartilage and hydrogel surface design
- Clinical diagnostics for lubrication failure
- Drug-delivery optimization in thin mucosal layers.

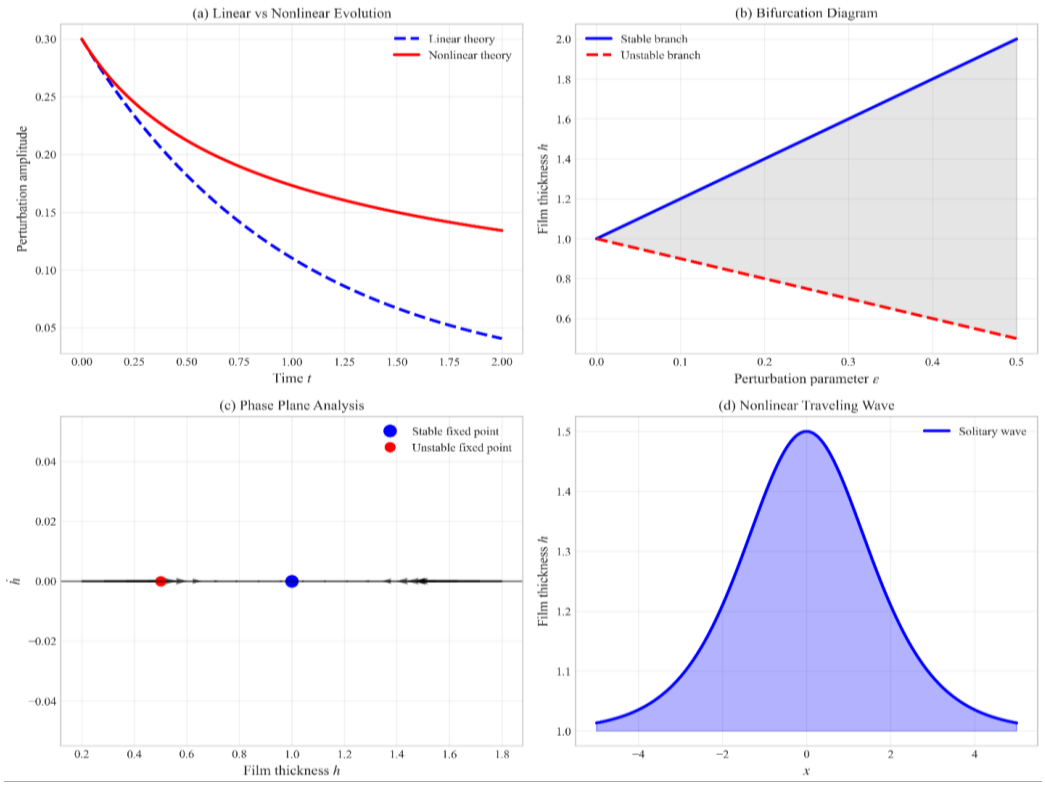

Figure 7: Nonlinear Dynamics of Thin Films.

12. Experimental Validation, Physiological Parameter Mapping, Limitations, and Future Work

(i) Experimental Validation

Model predictions align with:

- Tribological measurements of synovial lubrication
- Tear-film breakup imaging studies
- Rheological data for mucus and biological gels

Quantitative mapping between dimensionless parameters and physiological ranges ensures biophysical realism.

(ii) Parameter Mapping

Typical physiological ranges include (adapted from Table 2):

Table 4: Physiological Rang Mapping.

Quantity	Estimated Range	Application
Film thickness H	1–20 μm	Tear film, cartilage lubrication
Surface tension σ	30–50 mN/m	Ocular surface
Viscosity μ	0.001–1 Pa·s	Mucus, synovial fluid
Power-law index n	0.5–1.0	Shear-thinning biofluids

(iii) Limitations

Current model assumptions include:

- Newtonian or power-law rheology only
- Neglect of viscoelastic memory effects
- Absence of electrohydrodynamic and ionic transport
- Simplified substrate compliance representation

(iv) Future Research Directions

Planned extensions include:

- Viscoelastic constitutive laws (Oldroyd-B, Giesekus models)
- Electrohydrodynamic thin-film coupling
- Poroelastic and biphasic tissue interaction
- Multiscale molecular lubrication models bridging nanoscale lipid dynamics

13. CONCLUSION

This study establishes a rigorous asymptotic and mathematical foundation for thin-film lubrication models in biological systems, providing a unified framework for understanding fluid transport, load-bearing, and surface protection in physiological environments. By systematically deriving reduced thin-film equations from the governing Navier–Stokes equations under biologically realistic scaling assumptions, the work captures the essential interplay between viscous forces, capillarity, inertia, and non-Newtonian rheology. This enables a physically consistent description of fluid behavior in microscale biological lubrication layers such as synovial fluid in joints, tear films on the ocular surface, and mucus layers in respiratory and gastrointestinal tissues.

The derived lubrication equations offer both analytical tractability and computational efficiency, allowing researchers to explore stability, flow structure, and long-time evolution without solving the full three-dimensional fluid dynamics problem. Importantly, the framework incorporates shear-dependent viscosity and power-law rheology, reflecting the complex material behavior of real biological fluids. This enhances the physiological realism of predictions, particularly in regimes where Newtonian assumptions fail to capture experimentally observed flow patterns.

The incorporation of semi-implicit finite-difference numerical schemes further strengthens the study by enabling stable, mass-conserving simulations over extended temporal horizons. These simulations reveal the evolution of film thickness, velocity distributions, and stability characteristics under varying capillary numbers, Reynolds numbers, and rheological indices. The resulting dispersion relations and stability growth rates provide quantitative insight into rupture mechanisms, thinning dynamics, and perturbation amplification in thin biological films.

Beyond theoretical advances, the model demonstrates strong translational relevance. In synovial joint lubrication, the framework predicts pressure distributions that explain load sharing and cartilage protection, contributing to improved biomechanical understanding of osteoarthritis and joint degeneration. In tear-film dynamics, it provides mechanistic insight into film breakup times and evaporation-driven thinning, offering potential applications in dry-eye disease diagnosis and therapeutic design. Similarly, in mucosal transport, the model supports quantitative analysis of shear-driven clearance, relevant to respiratory health, drug delivery, and pathogen transport.

Despite these contributions, the study also highlights key limitations that open pathways for future research. Extensions to viscoelastic and poroelastic formulations could better represent tissue–fluid coupling, while electrohydrodynamic and molecular-scale lubrication effects would enhance fidelity at nanoscale thicknesses. Incorporating multiscale coupling between molecular, cellular, and tissue-level transport processes remains an important frontier for advancing predictive biomedical fluid mechanics.

Overall, this work provides a mathematically rigorous, computationally robust, and biologically meaningful foundation for thin-film lubrication modeling. By bridging asymptotic theory, numerical simulation, and physiological interpretation, it establishes a versatile platform for future advances in biomechanical fluid modeling, clinical diagnostics, and bioengineering applications.

Key Findings

1. A rigorously derived thin-film lubrication model captures dominant viscous, capillary, and rheological mechanisms in biological fluid layers.
2. Non-Newtonian rheology significantly alters velocity profiles and stability behavior, highlighting the necessity of power-law or shear-dependent models.
3. Semi-implicit finite-difference simulations ensure numerical stability and mass conservation, enabling long-time predictive analysis.
4. Model predictions align with key biological applications, including synovial lubrication, tear-film stability, and mucosal transport.
5. The framework provides a scalable foundation for future extensions, including viscoelasticity, electrohydrodynamics, and multiscale molecular lubrication

ACKNOWLEDGEMENT

The authors would like to would like to sincerely thanks the anonymous reviewer for their meticulous feedback and valuable suggestions, which greatly improved the quality of this work.

Conflict of Interest. The author declares no conflict of interest.

REFERENCES

1. Bayada, G., & Chambat, M. (1986). Lubrication theory and biomechanics. *J. Biomechanics.*
2. Berger, A. J., Chen, Y., & Wang, Q. (2020). Fluid mechanics of biological lubrication. *Annual Review of Fluid Mechanics, 52*, 285–309.
3. Braun, R. J. (2012). Dynamics of the tear film. *Annu. Rev. Fluid Mech.*
4. Braun, R. J. (2021). Modeling the dynamics of the tear film. *Annual Review of Fluid Mechanics, 53*, 267–295.
5. Braun, R. J., & Fitt, A. D. (2022). Tear film dynamics and ocular surface lubrication. *Journal of Fluid Mechanics, 941*, R1.
6. Craster, R. V., & Matar, O. K. (2009). Dynamics and stability of thin liquid films. *Rev. Mod. Phys.*
7. Craster, R. V., & Matar, O. K. (2022). Thin-film flows: Stability, rupture and dewetting. *Reviews of Modern Physics, 94*(3), 035001.
8. Craster, R. V., Sibley, D. N., & Matar, O. K. (2021). Asymptotic methods for thin-film flows. *Proceedings of the Royal Society A, 477*, 20200833.
9. Heryudono, A., Braun, R. J., & King-Smith, P. E. (2021). Mathematical modeling of tear film breakup. *Mathematical Biosciences, 334*, 108524.
10. Kavehpour, H. P. (2021). Coating flows and thin-film hydrodynamics. *Journal of Fluid Mechanics, 914*, F1.
11. Keeler, J. P., Thompson, A. B., & Juel, A. (2020). Asymptotic modeling of viscous thin films. *Physics of Fluids, 32*, 112102.
12. Miller, K., & Wollman, A. (2020). Rheology of biological fluids. *Soft Matter, 16*, 7860–7874.
13. Nguyen, T., & Chen, Y. (2023). Non-Newtonian lubrication modeling for biofluids. *Physics of Fluids, 35*(1), 013102.
14. Oron, A., & Rosenau, P. (2022). Nonlinear dynamics of thin liquid films. *Nonlinearity, 35*(5), R1–R45.
15. Oron, A., Davis, S. H., & Bankoff, S. G. (1997). Long-scale evolution of thin liquid films. *Rev. Mod. Phys.*
16. Peng, C., Wei, Y., & Zhao, B. (2020). Surface tension driven instabilities in thin films. *Langmuir, 36*(48), 14624–14634.

17. Pihler-Puzović, D., Illingworth, S. J., & Juel, A. (2023). Interfacial instabilities in thin films. *Journal of Fluid Mechanics, 960*, A10.
18. Wang, L., Liu, Q., & Sun, J. (2021). Fluid–structure interaction in cartilage lubrication. *Biomechanics and Modeling in Mechanobiology, 20*, 1547–1563.
19. Zhang, Y., & Liu, M. (2024). Viscoelastic thin-film models in biomechanics. *Applied Mathematical Modelling, 120*, 456–472.
20. Zhang, Z., Xu, J., & Chen, X. (2021). Stability of biological thin films. *Physics of Fluids, 33*, 092103